Application of Boost Converter to Increase the Speed Range of Dual-stator Winding Induction Generator in Wind Power Systems

Kavousi, Ayoub; Fathi , S. Hamid ; Milimonfared, Jafar; N. Soltani, Mohsen

Link to publication from Aalborg University

Application of Boost Converter to Increase the Speed Range of Dual-stator Winding Induction Generator in Wind Power Systems

Ayoub Kavousi, S. Hamid Fathi, *Member, IEEE,* Jafar Milimonfared, *Member, IEEE*, Mohsen N. Soltani, *Senior Member, IEEE*

Abstract—In this paper, a topology using a Dual-stator Winding Induction Generator (DWIG) and a boost converter is proposed for the variable speed wind power application. At low rotor speeds, the generator saturation limits the voltage of the DWIG. Using a boost converter, higher DC voltage can be produced while the DWIG operates at Maximum Power Point Tracking (MPPT) even at low speed and low voltage conditions. Semiconductor Excitation Controller (SEC) of the DWIG utilizes Control-Winding Voltage Oriented Control (CWVOC) method to adjust the voltage, considering *V/f* characteristics. For the proposed topology, the SEC capacity and the excitation capacitor is optimized by analyzing the SEC reactive current considering wind turbine power-speed curve, *V/f* strategy, and the generator parameters. The method shows that the per-unit capacity of the SEC can be limited to the inverse of DWIG magnetizing reactance per-unit value. The topology is simulated in MATLAB/Simulink platform and experimented with a scaled 1 kW prototype. Both simulation and experimental results demonstrate wide variable speed operation range of the DWIG and verify the optimization.

Index Terms—Boost converter, control-winding voltage oriented control, dual-stator winding induction generator (DWIG), Wind power, Variable speed operation.

I. INTRODUCTION

NOWADAYS, wind power generation is considered as an alternative to the conventional fossil fuel power plants. It is attracting more attention, as more than half of the present wind turbine capacity has been installed in the past five years [1]. The early wind turbine technology was based on squirrel-cage induction generators (SCIG), connected directly to the grid, therefore, the rotor speed remains almost constant. In the modern wind turbine technologies, due to the maximum wind power extraction and the gearbox problems, turbine designers preferred variable speed generator systems. Power electronic converters facilitate variable speed operation of the generators, which can also be employed in the wind power systems [2]-

A. Kavousi, S. H. Fathi and J. Milimonfared are with the department of Electrical Engineering, Amirkabir University of Technology, Tehran 4413-15875, Iran(emails: akavoosi@aut.ac.ir, fathi@aut.ac.ir, monfared@aut.ac.ir).
M. N. Soltani is with the department of Energy Technology, Aalborg University, Esbjerg, Denmark (email: sms@et.aau.dk).

[3]. Most of the variable speed wind turbine systems are based on Doubly-Fed Induction Generator (DFIG) or Permanent Magnet Synchronous Generator (PMSG) [4]-[5]. The PMSG-based wind turbine has a higher power density and efficiency; while suffering from the high cost of generator raw materials and the full-rated converter price. Instead, the DFIG-based systems have lower efficiency and higher maintenance costs due to the slip-ring and brush arrangement, but the generator and partial-rated converter price are lower [6].

Due to the environmental concerns and social/political restrictions, there is a growing demand for the offshore wind turbine installation, where better wind condition is also an advantage [7]. For the large-scale offshore wind farms that are placed far from the shore, the economical transmission system is High Voltage Direct Current (HVDC) transmission [8]. To integrate the wind turbines with HVDC transmission system, several promising solutions have been proposed in the literature [8]-[12]. In those studies, the integration of both DFIG and PMSG-based wind turbines with HVDC has been discussed. For the application, the DFIG-based system requires additional AC/DC converter which increases the investment cost. Moreover, the maintenance cost for DFIG in offshore wind farms is higher [10]-[11]. Although the investment cost for the PMSG-based wind turbine is high, the generators with DC output voltage are highly recommended to be integrated with HVDC system due to the higher efficiency, higher Annual Energy Production (AEP), lower maintenance costs and no need for additional AC/DC converter [8] and [12].

In recent years, Dual-stator Winding Induction Generator (DWIG) DC generation system has been proposed in the literature for the variable speed applications such as offshore wind power system, ship propulsion, and aircraft generation system [13]-[14]. In this context, various topologies of the DWIG generation system [15]-[16], control methods [17]-[19], and the system parameters design and optimization [20]-[21] have been explored. Additionally, some literature discusses the operation of DWIG under unbalanced load [22]-[23] and rotor-speed stability under fault condition [24]. The studies show that DWIG DC generation system achieves a reliable performance under various load and speed conditions and has several advantages such as high power density, robustness, innate overload protection, brushless construction,

less maintenance, and lower generator costs [24]-[26]. Therefore, the DWIG-based system can be considered as an attractive candidate for the wind power generators, especially for offshore HVDC windfarm, bringing about the reduction of the CAPital EXpenditure (CAPEX) and OPerating EXpenditure (OPEX).

In a wind power system, the generator's wide operating speed range is very beneficial to adopt wide wind speed variations and extract the wind power efficiently. The wide speed range operation for DWIG generation system has been investigated in the literature [21],[26]-[30]. Some of the studies discuss the operation, control and SEC optimization at the speed range 1-2 p.u. in which the rated speed is 4000 rpm. Generation at this speed range is suitable for high-speed applications such as aircraft generators, however, for a wind turbine, operation at lower speeds, especially lower than the rated speed, is required. In [28], DWIG generation system is proposed for the wind power application, and shows that the generator can operate in a speed range of 0.66-1.6 p.u. with the rated speed of 750 rpm. At the lower speeds, generator saturation acts as a limiting factor for the DWIG and prevents the output DC voltage to reach the nominal value. The wide speed range operation of DWIG for a wind system has been proposed in [29] and the grid-connected application of the topology has been presented in [30]. In these papers, to overcome the problem of generator saturation, the SEC controller mode is changed at low speeds and the SEC DC-link is connected to the output DC-link via a diode to supply the load. With this strategy, the capacity of SEC must be increased for active power flow at low speeds to achieve the speed range 0.4-1.6 p.u. On the other hand, changing the controller mode and power flow between the control-winding and power-winding cause a step change in the current of both windings. Also, another control process must be applied to switch the power flow by changing the DC voltage. Therefore, when there is some fluctuation in the generator speed, many transients are occurred. This may cause DC voltage and current oscillations, especially, at low wind and high turbulence conditions.

Structure of the diode rectifier and the boost converter with only one active switching element has several advantages such as simplicity, lower cost, reliability, and robustness, especially in high power applications [31]. The topology is used in the wind turbine systems either with PMSG or electrically excited synchronous generators (EESG) for MPPT control in variable speed range and to connect the higher voltage level [31]-[33]. But in the SCIG application of the topology, it suffers from reactive power supplement required for the generator excitation. In DWIG, the control-winding performs the generator excitation, providing the possibility of using a passive rectifier together with a boost converter, to control the generator active power and increase the voltage level at different speeds.

This paper proposes a topology in which a boost converter is utilized with the DWIG generation system to broaden the DWIG speed range to 0.2- 1.3 p.u. associated with a control system to track the maximum power point (MPP). Unlike the previous methods which try to regulate the power-winding DC-bus voltage within the operating speed range, in the proposed structure, the DC-bus voltage is allowed to be variable and the active power of the power-winding is regulated instead. Therefore, V/f strategy can be performed by the SEC at low speeds without the need to change the control mode and switch the power flow between power and control windings. In the topology, to adjust the DWIG voltage in the speed range, Control-Winding Voltage Oriented control (CWVO) is employed by the SEC while V/f characteristic of the DWIG is considered. In this paper, the optimization of SEC capacity and the excitation capacitor is also modified based on the proposed topology while the power-speed curve of the wind turbine and V/f strategy for DWIG voltage control are considered. Finally, wide-speed-range operation and optimization of the system are verified by computer simulation and experimental results.

II. PROPOSED TOPOLOGY

In the wind power application, to ensure that the wind turbine tracks the maximum power point (MPP), variable speed operation is required. Particularly, in low wind speed condition, to increase the output power, the generator must work at low speed, to increase the blade aerodynamic efficiency. This operation increases the annual energy output and decreases the time period of investment return [34]. Fig. 1 shows the wind turbine power-speed curves for various wind speeds in which each curve has its MPP at a specified speed. So, one of the main objectives of the control system is to adjust the generator speed at the optimal value.

In this paper, a boost converter is utilized in the DWIG-based system to control the generator speed for MPPT purpose in a wide speed range. The proposed topology is shown in Fig. 2. The topology employs a squirrel cage induction generator with two sets of stator windings, wounded in the same stator slots and both are star-connected 3-phase winding with the same number of poles. One is the control-winding, which is used to control the generator excitation and supply a part of generator reactive power. The other is power-winding used for active power generation. Nevertheless, some part of the generator reactive power is provided through the power-winding by the excitation capacitor (C_{exc}).
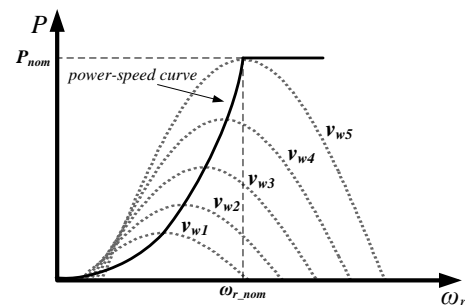

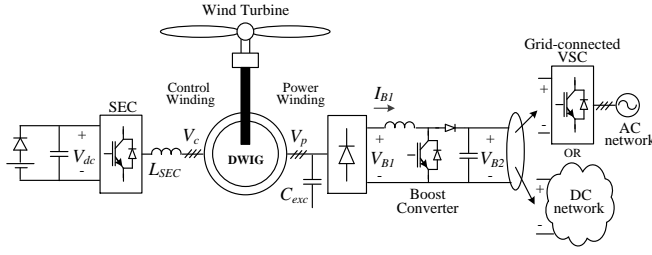Fig. 1. Wind turbine power-speed curve at different wind speeds (v_w).

Fig. 2. Proposed topology.

In the control-winding side, a voltage source converter, named SEC, is connected to the winding via a coupling inductor (L_{SEC}). Also, a low voltage battery with a series diode is connected to DC side of SEC to charge the capacitor for the system start-up. At normal operation, SEC regulates its DC-link voltage (V_{dc}) to a specific reference value, which is more than the battery voltage, so the diode is reverse biased. The main role of SEC is regulation of the control-winding voltage. Meanwhile, the frequency is controlled according to the generator speed and the slip frequency which is imposed by the load. To generate electrical energy at the low-speed conditions, where the frequency is low, magnetic saturation of the generator is the main limitation. In such condition, the SEC decreases the amplitude of the control-winding voltage according to *V/f* strategy to avoid saturation.

In the power-winding side, there is a 3-phase diode rectifier and an excitation capacitor. The output DC-link of the diode rectifier is directly connected to a boost converter. The diode rectifier converts the variable amplitude and frequency voltage of the power-winding into a DC voltage (V_{B1}), and then the boost converter adjusts the output power at the MPP, according to the power-speed curve. This can be performed by controlling the boost converter input current (I_{B1}), which leads to the control of the generator power-winding current, as well as the generator power. The output voltage of the boost converter is regulated at a higher constant value by a grid-connected converter to inject the generated power to the AC network. In addition, the boost converter output can be connected to a DC network with a higher voltage such as HVDC.

III. DWIG Model

The dynamic equations of the DWIG voltage equations in d-q frame, based on the method given in [35] can be expressed as (1):

$$
\begin{cases}
v_{cd} = R_c i_{cd} - \omega \lambda_{cq} + d\lambda_{cd}/dt \\
v_{cq} = R_c i_{cq} + \omega \lambda_{cd} + d\lambda_{cq}/dt \\
v_{pd} = R_p i_{pd} - \omega \lambda_{pq} + d\lambda_{pd}/dt \\
v_{pq} = R_p i_{pq} + \omega \lambda_{pd} + d\lambda_{pq}/dt \\
v_{rd} = R_r i_{rd} - (\omega - \omega_r)\lambda_{rq} + d\lambda_{rd}/dt = 0 \\
v_{rq} = R_r i_{rq} + (\omega - \omega_r)\lambda_{rd} + d\lambda_{rq}/dt = 0
\end{cases}
\tag{1}
$$

where ω and ω_r are the angular synchronous frequency and the rotor speed, and *v*, *i*, and *λ* refer to voltage, current and flux linkage respectively. The indices *c*, *p,* and *r* are related to

the control-winding, power-winding, and rotor parameters. In the model, both control and rotor winding parameters are transferred to the power-winding side. Both d and q axis voltages of the rotor-winding are zero, due to the squirrel cage type of the rotor. The linkage fluxes equations are described in (2):

$$
\begin{cases}
\lambda_{cd} = L_c i_{cd} + L_{cp} i_{pd} + L_{cr} i_{rd} \\
\lambda_{cq} = L_c i_{cq} + L_{cp} i_{pq} + L_{cr} i_{rq} \\
\lambda_{pd} = L_{pc} i_{cd} + L_p i_{pd} + L_{pr} i_{rd} \\
\lambda_{pq} = L_{pc} i_{cq} + L_p i_{pq} + L_{pr} i_{rq} \\
\lambda_{rd} = L_{rc} i_{cd} + L_{rp} i_{pd} + L_r i_{rd} \\
\lambda_{rq} = L_{rc} i_{cq} + L_{rp} i_{pq} + L_r i_{rq}
\end{cases}
\tag{2}
$$

where the inductances are:

$$
\begin{cases}
L_c = L_{lc} + L_{lcp} + L_m \\
L_p = L_{lp} + L_{lcp} + L_m \\
L_r = L_{lr} + L_m \\
L_{cp} = L_{pc} = L_{lcp} + L_m \\
L_{cr} = L_{rc} = L_m \\
L_{pr} = L_{rp} = L_m
\end{cases}
\tag{3}
$$

in which, L_{lc}, L_{lp} and L_{lr} are the control-winding, power-winding and rotor-winding leakage inductance, respectively, and L_m refers to the magnetizing inductance. The mutual leakage inductance between control and power windings (L_{lcp}) can be neglected because of its insignificant value. Fig. 3 shows the equivalent d-axis and q-axis circuit models of the DWIG.

(a)

(b)

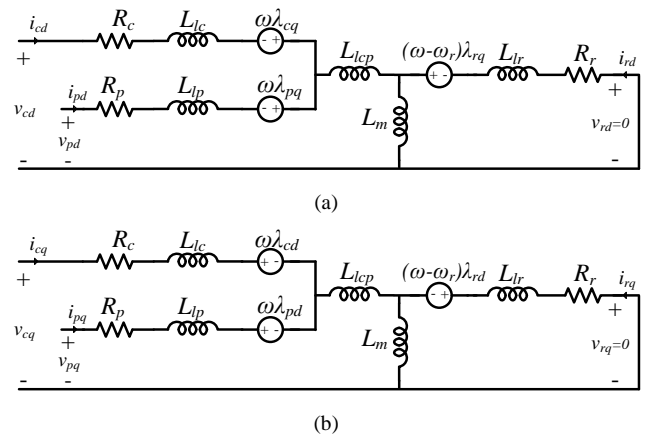Fig. 3. Circuit model of the DWIG a) d-axis, b) q-axis.

IV. Control Strategy

A. DWIG excitation control strategy

In this paper, adjusting the control-winding voltage (V_c) is the main role of SEC to excite the DWIG. Since in the proposed topology, the boost converter is used to increase the output voltage level, *V/f* strategy can be applied in the DWIG excitation controller for low-speed generation. For this

purpose, the SEC DC-link voltage (V_{dc}) must be regulated at a reference value. In this paper, to adjust the V_c and V_{dc}, CWVO strategy is employed. Fig. 4 shows the block diagram of CWVO control strategy for DWIG.
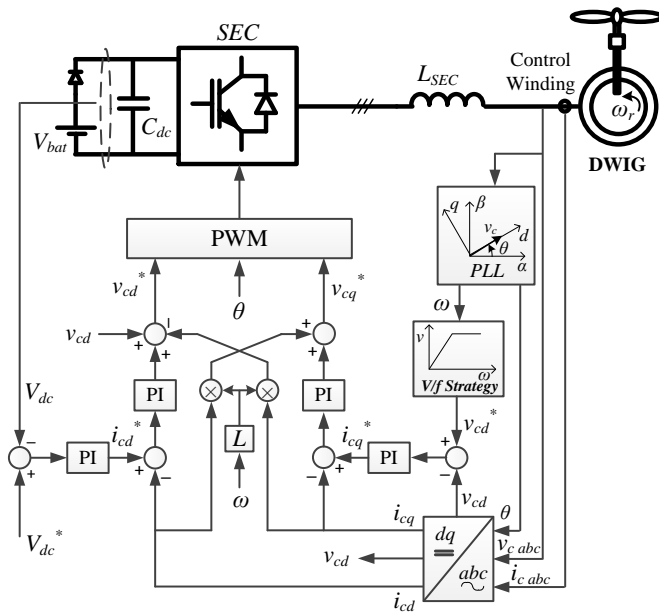

Fig. 4. DWIG CWVO excitation control strategy.

In this method [16], aligning the control-winding voltage with the d-axis, the q-axis voltage (v_{cq}) becomes zero and the d-axis voltage (v_{cd}) equals the amplitude of the control-winding voltage as in (4):

$$\begin{cases} v_{cd} = |V_c| \\ v_{cq} = 0 \end{cases} \tag{4}$$

Therefore, according to the instantaneous power theory [36], the control winding active power (p_c) and reactive power (q_c) are:

$$\begin{cases} p_c = \dfrac{3}{2} v_{cd} i_{cd} \\ q_c = -\dfrac{3}{2} v_{cd} i_{cq} \end{cases} \tag{5}$$

For v_{cd} in (1), if the voltage drop across the winding resistance ($R_c i_{cd}$) is neglected and the control-winding d-axis flux is assumed to be constant ($d\lambda_{cd}/dt=0$), then:

$$v_{cd} \simeq -\omega\lambda_{cq} \tag{6}$$

and (4) can be modified as:

$$\begin{cases} p_c \simeq -\dfrac{3}{2} \omega\lambda_{cq} i_{cd} \\ q_c \simeq +\dfrac{3}{2} \omega\lambda_{cq} i_{cq} \end{cases} \tag{7}$$

which shows that the control-winding active and reactive power can be controlled by i_{cd} and i_{cq} respectively.

The power balance relationship between the SEC DC-link

and control-winding can be expressed as in (8):

$$\frac{\partial(\frac{1}{2} C_{dc} V_{dc}^2)}{\partial t} + p_{SEC\_loss} = -p_c \tag{8}$$

where C_{dc} and p_{SEC_loss} are the SEC DC-link capacitor and power loss respectively. Similar to a Static Synchronous Compensator (STATCOM), SEC absorbs a little active power for its internal power loss, when exchanging reactive power; otherwise, the DC-link voltage would not be stable. Therefore, V_{dc} can be controlled by the control-winding active power.

As described in [21], the control-winding flux (λ_{cq}) can be regulated by control-winding reactive power (q_c) at different speeds. This can be presented by (9) using the equations of λ_{cq} and q_c, given in (2) and (7) respectively:

$$\lambda_{cq}.\lambda_{ccq} = q_c.L_s / \omega \tag{9}$$

where λ_{ccq} is a part of the control-winding flux λ_{cq}, induced by i_{sq} in the control-winding. On the other hand, (4) and (6) show that by regulating the control-winding q-axis flux (λ_{cq}), the amplitude of control-winding voltage can be adjusted. Therefore considering (7), (8), and (9), it can be expressed that:

$$\begin{cases} i_{cd} \Rightarrow p_c \Rightarrow V_{dc} \\ i_{cq} \Rightarrow q_c \Rightarrow \lambda_{cq} \Rightarrow V_c \end{cases} \tag{10}$$

Equation (10) indicates that in the proposed system, control of the SEC DC-link voltage (V_{dc}) and control-winding voltage (V_c) can be performed by the control of i_{cd} and i_{cq} respectively.

In DWIG excitation control strategy as shown in Fig. 4, the controller uses a decoupling strategy with PI controllers in current loop, to control i_{cd} and i_{cq} separately and independent of the DWIG parameters [19]. To determine the control-winding d-axis reference current (i_{cd}^*), V_{dc} is compared with its reference value and the output error is passed through a PI controller. Similarly, the q-axis reference current (i_{cq}^*) is obtained by comparing V_{cd} with its reference value and using another PI controller. At low-frequency operation, corresponding to low generator speed, V/f strategy is applied, i.e. V_{sd}^* is determined according to the operating frequency.

B. Boost converter MPPT control

As the excitation control regulates the DWIG voltages, the boost converter controls the generator active power based on MPPT. The boost converter provides a wide speed range of operation, including low-speed condition, where the DWIG voltage is reduced according to V/f strategy. Boost converter accommodates the increase in the output voltage and connects the generator to a higher voltage level. For MPPT, the control strategy presented in [32] is employed. The control scheme for the boost converter is shown in Fig. 5.
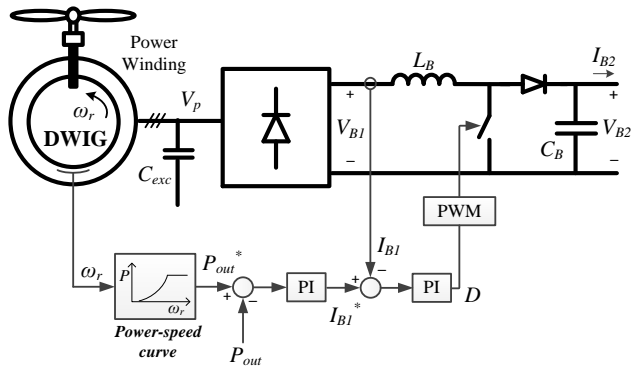
Fig. 5. Boost Control strategy for MPPT operation.

To achieve MPPT, the controller uses a look-up table, which is obtained from the power-speed curves presented in Fig. 1. In the look-up table, for any given DWIG speed (ω_r), the optimum power (P_{out}^*) is stored. The optimum power is considered as reference power in the boost controller to adjust the output power at MPP. If the boost converter power loss is ignored, the output power (P_{out}) can be obtained from (11):

$$P_{out} = V_{B2}I_{B2} \simeq V_{B1}I_{B1} \tag{11}$$

V_{B1} can be written as a constant ratio of power-winding voltage if the diode rectifier voltage drop is ignored. Since the DWIG control and power windings experience the same air gap flux, controlling the voltage of control-winding leads to regulation of power-winding voltage. Therefore, the power-winding voltage can be replaced by the control-winding voltage considering the voltage drop across the generator impedance. The voltage drop depends on the control-winding and power-winding currents which are determined by control-winding voltage and rectifier/boost converter current. So, V_{B1} and P_{out} can be expressed by (12) and (13), respectively:

$$V_{B1} = \frac{3\sqrt{2}}{\pi}.U_p = \frac{3\sqrt{2}}{\pi}.\frac{n_p}{n_c}.U_c - \Delta U(I_{B1}, U_c) \tag{12}$$

$$P_{out} = \left(\frac{3\sqrt{2}}{\pi}.\frac{n_p}{n_c}.U_c - \Delta U(I_{B1}, U_c) \right).I_{B1} \tag{13}$$

Where U_p and U_c denote the line voltage of power-winding and control-winding respectively; ΔU is the voltage drop across control-winding and power-winding; n_p/n_c is the turn ratio of the windings. Since U_c is regulated by the excitation control to its reference value, P_{out} - given in (13)- can be controlled by I_{B1}. So in the power regulation loop, P_{out} is compared with its reference value and using a PI controller, the reference value of I_{B1} is obtained. In the current regulation loop, I_{B1} is compared with its reference value and the output error is passed through another PI controller to determine the duty cycle (D) of the boost converter. Finally, using PWM technique with saw-tooth carrier waveform, the duty cycle is converted to the switch drive signal.

V. OPTIMIZING THE SEC CAPACITY AND EXCITATION CAPACITOR

Within the wide speed range operation of DWIG, tracking the required reactive current at different loads and speeds is the most important issue in order to determine the capacity of SEC and the optimum excitation capacitor. The required reactive current is partially supplied by SEC and the rest is supplied by the excitation capacitor. At low-speed generation where the frequency is low, the excitation capacitor current is not significant and SEC supplies most of the generator reactive current. As speed rises, the generator load is increased due to the wind turbine power-speed curve. In this condition, the generator needs more reactive current. Besides, the frequency rise leads to increase in the capacitor current. Therefore, if C_{exc} is properly selected, the SEC reactive current can be limited to its low-speed generation value and the capacity of SEC can be minimized. In this paper, this optimization is performed based on the wind turbine power-speed curve while *V/f* strategy is considered.

A. Determining the control-winding current at different speeds

For a sinusoidal and balanced condition, the simplified per phase equivalent model of the proposed system and its phasor diagram are shown in Fig. 6. In the model, it is assumed that 1) the fundamental components of the currents are considered and harmonics are neglected, 2) the mutual leakage inductance between the control-winding and the power-winding is neglected, 3) SEC and boost converter power loss and DWIG hysteresis and eddy loss are ignored, 4) SEC generates only reactive current aligned with DWIG magnetizing current.
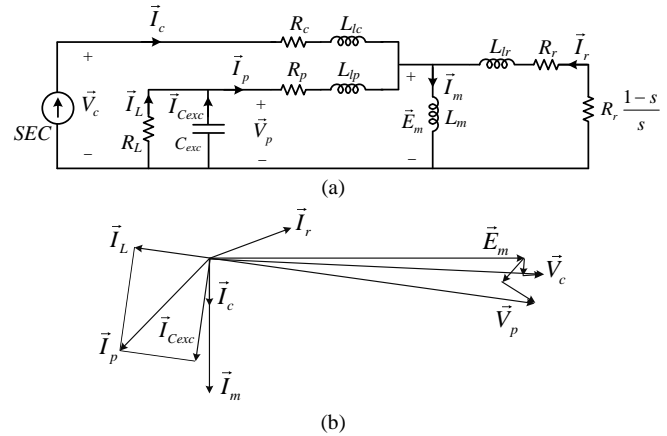
Fig. 6. a) Per phase circuit diagram of DWIG. b) DWIG phasor diagram.

In Fig. 6(a), SEC is modeled as a current source which regulates the control-winding voltage by controlling the SEC current. The rectifier and boost converter is considered as a load resistor (R_L) which varies based on the power-speed curve of the turbine and determines the rectifier input current (IL). At steady state, this current can be calculated uniquely for different rotor speeds as it is described in [28]:

$$I_c = \frac{E_m}{X_m} + \frac{E_m X_r}{(\frac{R_r}{s})^2 + X_r^2} + \frac{X_p(I_L^2 + I_{Cexc}^2)}{E_m} - \frac{V_p^2}{E_m X_{Cexc}} \qquad (14)$$

where X_m, X_p, X_r denote the magnetizing, power-winding, and rotor leakage reactance of the generator respectively. I_{Cexc} and X_{Cexc} are the excitation capacitor current and reactance and s is the DWIG slip and is defined as:

$$s = \frac{\omega - \omega_r}{\omega} \qquad (15)$$

In (14), E_m is the back electromotive force and it is assumed that V_c and E_m are approximately the same (i.e. $E_m \approx V_c$). On the other hand, V_c is regulated by SEC based on the *V/f* strategy, therefore, E_m can be defined as:

$$E_m(\omega) = \begin{cases} \frac{V_{cn}}{\omega_n} . \omega & , \quad \omega < \omega_n \\ V_{cn} & , \quad \omega \geq \omega_n \end{cases} \qquad (16)$$

where V_{cn} and ω_n are the nominal control-winding voltage and the nominal angular frequency of DWIG.

The first term in (14) is the reactive current consumed by DWIG magnetizing reactance and is the main reactive current required for DWIG operation. The second term denotes the reactive component of rotor current which depends on the DWIG load. The reactive current consumed by power winding reactance is the third term and the last term denotes the generated reactive current by the excitation capacitor. To compute I_c form (14), at first, some variables such as ω, s, V_p, and I_L must be calculated at different speeds:

1) Calculation of ω and s

Since the generator reactances and E_m in (15) are frequency dependent, it is essential to obtain the frequency at the corresponding rotor speed. The frequency and slip can be obtained according to the transmitted power from the rotor to the stator (P_e):

$$P_e = \frac{-3Rr}{s} . \frac{E_m^2}{(\frac{R_r}{s})^2 + X_r^2} \qquad (17)$$

Since DWIG operates at MPP, P_e follows the power-speed curve at different speeds. So, P_e can be defined as a function of speed:

$$P_e = F(\omega_r) \qquad (18)$$

where $F(\omega_r)$ is the power-speed curve presented in Fig.1. Substituting (15), (16) and (18) in (17), a nonlinear relationship between ω and ω_r is obtained and iteration method can be utilized to find ω, s versus ω_r.

2) Calculation of V_p and I_L

According to Fig. 6(a), V_p can be expressed in term of E_m:

$$V_p = \frac{E_m R_L}{\sqrt{(R_p + R_L - \frac{R_L.X_p}{X_{Cexc}})^2 + (X_p + \frac{R_L.R_p}{X_{Cexc}})^2}} \qquad (19)$$

and I_L is:

$$I_L = \frac{V_p}{R_L} = \frac{E_m}{\sqrt{(R_p + R_L - \frac{R_L.X_p}{X_{Cexc}})^2 + (X_p + \frac{R_L.R_p}{X_{Cexc}})^2}} \qquad (20)$$

to obtain V_p and I_L from (19) and (20), it is necessary to determine R_L which is the per-phase equivalent of the boost converter together with the rectifier, as shown in Fig. 7.
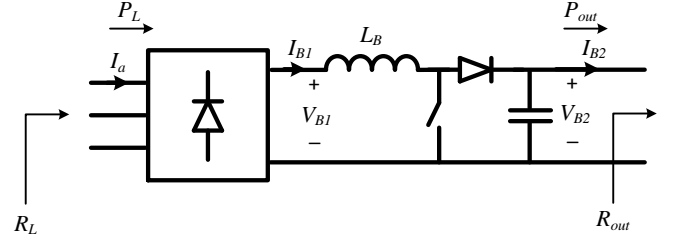

Fig. 7. Boost converter-rectifier and equivalent load resistance.

When the boost converter operates in continuous conduction mode, it can be shown that:

$$R_L = \frac{\pi^2 (1-D)^2}{18} R_{out} \qquad (21)$$

where R_{out} is the equivalent output resistance of the boost converter and D is the duty cycle. Since the boost converter output is connected to a regulated DC-link, V_{B2} is constant and R_{out} can be expressed in terms of V_{B2} and the boost converter output power (P_{out}), Therefore:

$$R_L = \frac{\pi^2 (1-D)^2 V_{B2}^2}{18 P_{out}} \qquad (22)$$

In addition, the active power transferred from DWIG terminal to R_L is:

$$P_L = 3\frac{V_p^2}{R_L} = \frac{3R_L E_m^2}{(R_p + R_L - \frac{R_L X_p}{X_{Cexc}})^2 + (X_p + \frac{R_L R_p}{X_{Cexc}})^2} \qquad (23)$$

Substituting (22) in (23) and neglecting the power loss in the rectifier, the boost converter (i.e. $P_{out} \approx P_L$), the duty cycle can be calculated as:

$$D = 1 - \frac{3X_{Cexc}}{\pi V_{B2}} \sqrt{\frac{3E_m^2 - 2R_p P_{out} + \sqrt{9E_m^4 - 12E_m^2 R_p P_{out} + 4R_p^2 P_{out}^2 - 4P_{out}^2 (R_p^2 + X_p^2)\frac{R_p^2 + (X_{Cexc} - X_p)^2}{X_{Cexc}^2}}}{R_p^2 + (X_{Cexc} - X_p)^2}} \qquad (24)$$

Substituting (24) in (22) and considering the power-speed curve as the boost converter output power, i.e. $P_{out} = F(\omega_r)$, R_L can be determined for different speeds. Therefore, V_p and I_L, which are required for the control-winding current calculation, can be obtained from (19) and (20).

B. Behavior of I_c vs ω_r using different C_{exc}

To show the control-winding current behavior, a 2.3 MW, 690V, 50Hz, 4pole DWIG system is studied. The generator parameters are described in [37] where the control winding and power winding have the same parameters. The rotor speed

range is considered between 0.2 p.u. and 1.3 p.u. of the base speed. Fig. 8(c) shows the behavior of I_c for different excitation capacitors. The currents are obtained based on the power-speed curve and V/f strategy which are respectively shown in Fig. 8(a) and (b). In Fig. 8(c), the curve with $C_{exc}=0$ shows the reactive current requirement of DWIG. This curve shows that I_c is increased as the speed and load rise. At the low-speed, low-load condition, the change in excitation capacitor has little effect on the control-winding current. In other words, the whole current at low-speed condition must be supplied by SEC. The value of this current is approximately equal to E_m/X_m, i.e. the first term in (14). Also, at high-speed operation, the bigger capacitance causes more decrease in the control-winding current. The reason is that the rotor speed rising leads to increase the voltage and frequency of the system, so the excitation capacitor can supply more reactive current for the generator requirement. At the speeds higher than $\omega_r=1.2$ p.u., the output power is kept constant and the required reactive current of DWIG is almost constant. On the other hand, as the speed increases, the capacitor reactive current is increased depending on the frequency. Therefore, the control-winding reactive current is decreased compared to its value at $\omega_r=1.2$ p.u. The slope of decrease is affected by the capacitor size, getting sharper with higher values of the capacitor.
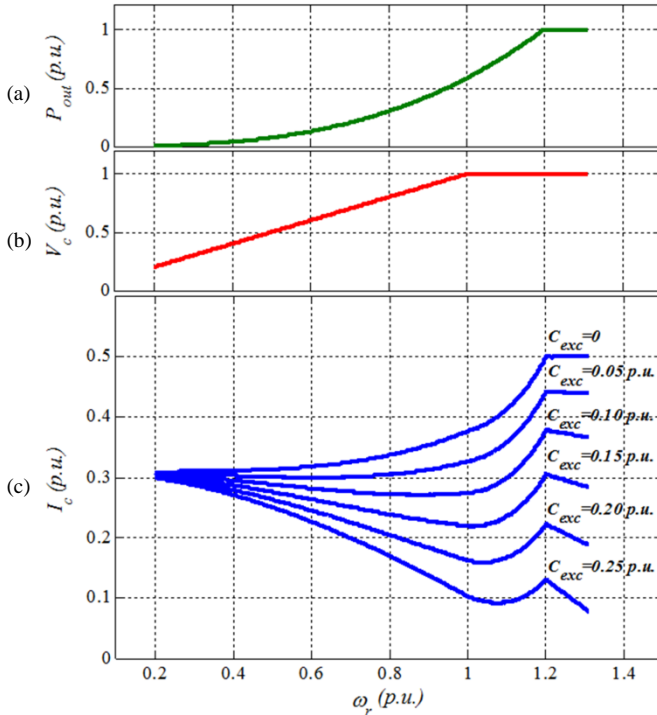

Fig. 8. a)Power speed curve b) Corresponding Vc vs speed. c) Calculated Control-winding current for different capacitors.

C. Excitation capacitor and SEC capacity calculation

Based on Fig. 8, if the capacitor is selected big enough, the maximum value of I_c can be limited to its value corresponding to the minimum speed. Although the bigger capacitor decreases the value of I_c at high rotor speeds, SEC capacity will not be affected. Thus, selecting minimum C_{exc} is cost

effective. The minimum capacitor can be selected based on (25):

$$I_c(\omega_{r\_min}) - I_c(\omega_r) \leq \varepsilon \qquad (25)$$

where ε is a small positive number. As it is seen in Fig. 9, at high speeds, the maximum value of I_c occurs at the rated speed (ω_{r_rated}) and (25) can be rewritten as:

$$I_c(\omega_{r\_min}) - I_c(\omega_{r\_rated}) \leq \varepsilon \qquad (26)$$

To obtain the optimum value of the excitation capacitor, an iterative method can be employed, taking (26) as the objective function. For the system under study, the optimum value for C_{exc} is obtained about 0.15 p.u.
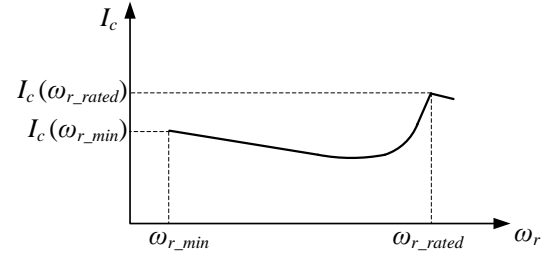

Fig. 9. The behavior of control-winding current in the different rotor speed.

The capacity of the SEC can be obtained as follows:

$$S_{SEC(p.u.)} = \max\left\{V_{c\,(p.u.)}\right\} \cdot \max\left\{I_{c\,(p.u.)}\right\} \qquad (27)$$

The maximum value for $V_{c(p.u)}$ is 1p.u. which is the nominal voltage of the control-winding. By selecting the optimum C_{exc}, the maximum value of I_c will be its value at minimum speed:

$$\max\left\{I_{c\,(p.u.)}\right\} \simeq \left. \frac{V_{c(p.u)}}{\omega L_{m(p.u)}}\right|_{\omega=\omega_{min}} \qquad (28)$$

The voltage to frequency ratio is taken constant and equal to 1 p.u. when the frequency is lower than its base value, then (27) can be simplified to:

$$S_{SEC(p.u.)} \simeq \frac{1}{L_{m(p.u)}} \qquad (29)$$

Equation (29) can be deduced such that per-unit capacity of SEC can be limited to the inverse of the magnetizing inductance per-unit value. For the 2.3MW DWIG, with magnetizing inductance about 3.24 p.u., SEC capacity is obtained 30 percent of the base MW.

VI. SIMULATION RESULTS

Using MATLAB/Simulink platform, DWIG system is simulated to evaluate its performance and study the effect of optimal excitation capacitor. Simulation results are obtained for the 2.3MW DWIG system introduced in section V. In the system, the boost converter output is connected to the grid via a 3-pahase voltage source converter. C_{exc} is set to 0.15 p.u., as obtained in the previous section.
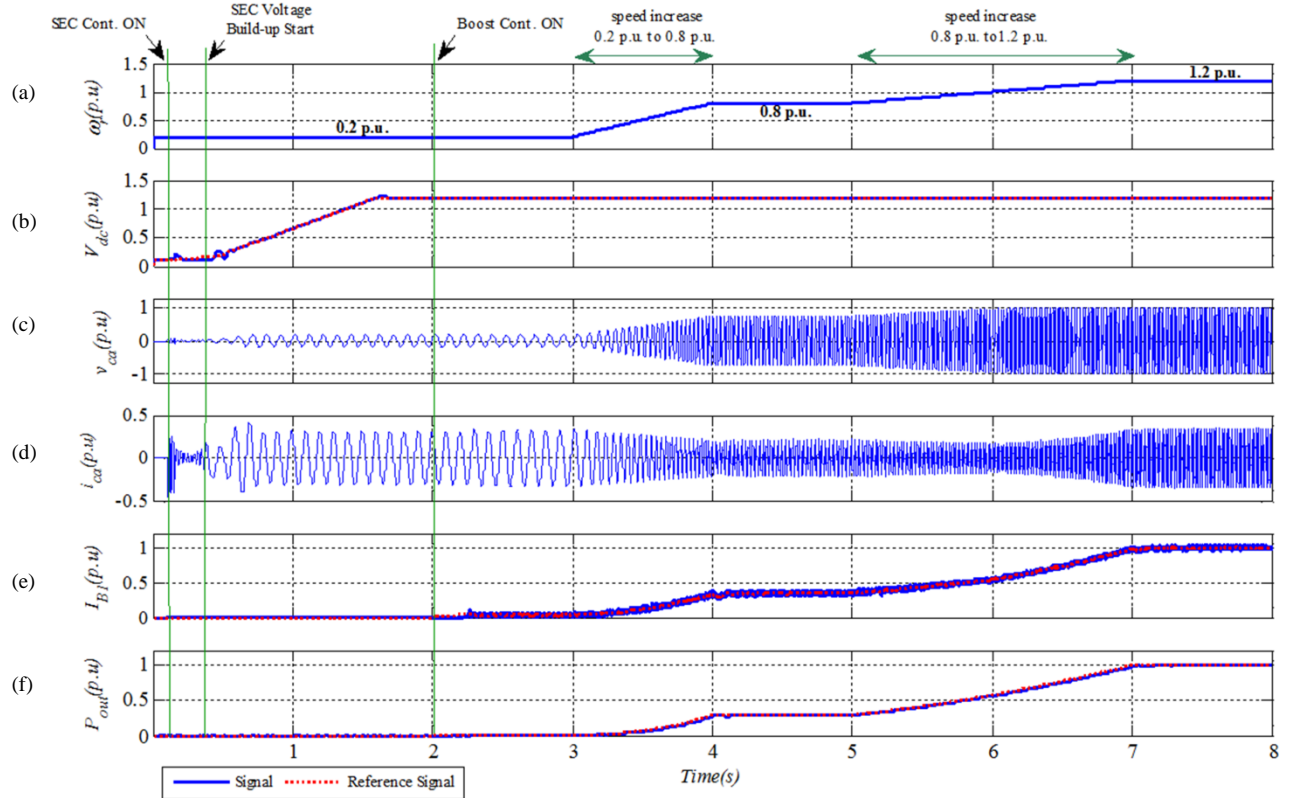
Fig. 10. Simulation result of 2.3MW DWIG.

Fig. 10 shows the simulation result of the DWIG system. At t = 0.1 s, the SEC controller is activated and at t = 0.4 s, the SEC DC-link voltage (V_{dc}) and control-winding voltage (V_c) starts to build up. After SEC start-up process, at t = 2 s, the boost converter starts to control the output power based on the power-speed curve. As it is seen in Fig. 10(a), at t = 3 s and t = 5 s, the prime mover starts to increase the rotor speed from 0.2 p.u to 0.8 p.u. and from 0.8 p.u. to 1.2 p.u., respectively.

Fig. 10(b) shows that V_{dc} follows its reference signal to reach its nominal value of 1.2 p.u. As indicated in the figure, the voltage is well controlled with increasing DWIG speed and load. The phase-A voltage of the control-winding (v_{ca}) is shown in Fig. 10(c). During start-up process, because of the low-speed operation, the amplitude of the voltage is limited to about 0.2 p.u., to avoid DWIG magnetic saturation. With the speed rising, the voltage amplitude is increased as the frequency is increased. At speeds above 1 p.u., the controller adjusts the control-winding voltage to its nominal value (1 p.u.). Figs 10(b) and 10(c) show that DWIG excitation strategy has a good performance in control-winding voltage regulation.

In Fig 10.(d), the phase-A current of the DWIG control-winding (i_{ca}) is presented. As expected, the behavior of the current is similar to that presented in Fig. 8(c) when C_{exc} is selected 0.15 p.u. After SEC voltage build-up, at all speeds, the current is limited to 0.3 p.u., which shows properness of the excitation capacitor selection.

Figs 10(e) and 10(f) show the input current of the boost converter and the power injected into the grid by the voltage source converter, respectively. As indicated in the figures,

both variables follow their reference signals which are determined by the wind turbine power-speed curve. These figures prove the performance of the boost converter control strategy in tracking MPP.

The simulation results show that as the SEC controller excites DWIG, the output power control is performed properly at different speeds by the boost converter. Therefore, by using the boost converter in DWIG DC generation system, MPPT is achieved in a wide range of rotor speed.

VII. EXPERIMENTAL RESULTS

To verify operation of the proposed system in a wide speed-range and validity of the optimization method for SEC capacity and excitation capacitor, an experimental setup is developed as shown in Fig. 11. The platform consists of a 1 kW DWIG, coupled with a 2.85 kW DC motor as the prime mover, which is connected to a DC drive system to adjust the rotation speed. The main parameters of DWIG system are presented in Table I. The control-winding of DWIG is connected to the SEC via an 8 mH inductor and is controlled by a TMS320F2812 DSP control board. In DWIG power winding side, there is a 77 uF/phase excitation capacitor bank which is selected by the proposed optimization method and a 3-phase diode rectifier together with a boost converter. The boost converter control strategy is implemented by an STM32F407VGT6 ARM microcontroller. The DC-link output of the boost converter is tied to a grid-connected inverter which regulates the DC-link voltage to 200 V.

Fig. 11.Experimental setup of the DWIG system.

TABLE I
PARAMETERS OF THE DWIG SYSTEM

Quantity	Symbol	Value
Rated output power	P	1 kW
Rated control winding line voltage	U_c	230 V
Rated control winding line voltage	U_p	115 V
Pole pair	pp	2
Base frequency	f_b	50 Hz
Base rotation speed	N_b	1500 rpm
Rated rotation speed	N_n	1800 rpm
Power-winding resistance	R_p	1.52 Ω
Power-winding leakage inductance	Ll_p	4.9 mH
Control-winding resistance	$^*R_c$	2.48 Ω
Control-winding leakage inductance	$^*L_{lc}$	5.2 mH
Rotor resistance	$^*R_r$	1.63 Ω
Rotor leakage inductance	$^*L_{lr}$	5.6 mH
Magnetizing inductance	$^*L_m$	59.1 mH
Battery voltage	V_{bat}	48 V
SEC DC-link voltage	V_{dc}	400 V
SEC DC-Link capacitor	C_{dc}	560 uF
SEC coupling inductor	L_{SEC}	8 mH
Excitation Capacitor	C_{exc}	77 uF
Boost converter output voltage	V_{B2}	200 V
Boost converter inductor	L_B	10 mH
Boost converter capacitor	C_B	470 uF

*All the generator parameters are referred to power winding side.

During start-up process, the boost converter output DC voltage is regulated by the voltage source converter to 200 V and the prime mover adjusts the rotor speed to 300 rpm. When the rotor speed reaches 300 rpm, SEC DC-link voltage starts a ramp build-up toward the reference value. As shown in Fig. 12 (a), V_{dc} is ramped up to 400 V by the controller. In this situation, i_c includes a reactive component and also a small negative active component to charge the capacitor and supply SEC power loss. The reactive component supplies the required reactive power of DWIG for regulation of the control-winding voltage, which leads to increase V_{B1} as shown in Fig 12(b). After a transient, i_{ca} is limited to the required value, settled at 1.8 A as expected. Then, the boost converter initiates power generation according to the power-speed curve. Fig. 12(b) also shows when the boost converter begins to control, I_{B1} is increased to extract active power from DWIG and because of the voltage drop across power winding impedance, V_{B1} is slightly decreased. Before starting the boost converter, I_{B1} is zero, then the current increases so that the output power reaches to 5 W. These waveforms prove the proper operation of DWIG with boost converter at low-speed condition, which is beneficial for MPPT.
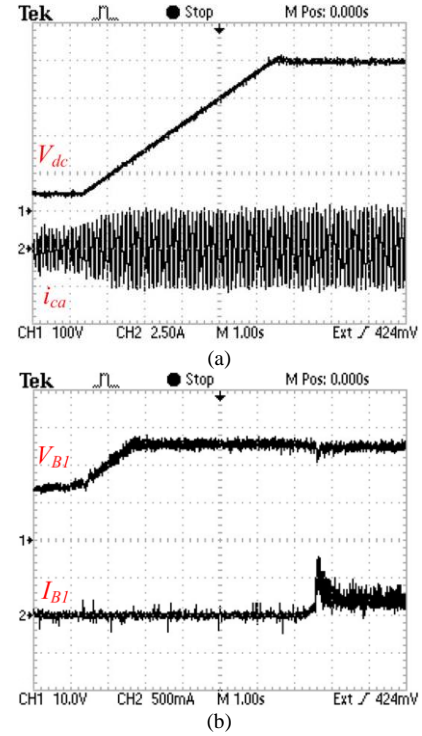

(a)

(b)

Fig. 12. Experimental result of the start-up process. a) V_{dc}, i_{ca}. b) V_{B1}, i_{B1}.

Fig. 13 shows the operation of the proposed topology when the rotor speed (N_r) is increased from 300 to 1800 rpm. Fig. 13(a)-(c) show the dynamic process for the speed increase from 300 rpm to 1200 rpm and Fig. 13(d)-(f) are related to speed increase from 1200 rpm to 1800 rpm. Fig. 13(a) indicates that with increasing speed from 300 rpm to 1200 rpm, i_{ca} decreases due to increase in excitation capacitor current by the frequency rise. At speeds above 1200rpm, i_{ca} decreases to the minimum value but then increases to the highest value at 1800 rpm as illustrated in Fig. 13(d). The behavior of i_{ca} in Fig.13(a) and (d), is the same as that shown in Fig. 8. Fig. 13(b) and (e) show that with increasing speed, the voltage V_{B1} is increased because V/f strategy is performed. Moreover, the current I_{B1} is increased by the boost converter controller to extract active power from DWIG. In Fig. 13(e), when the speed is above 1650 rpm, the frequency is above 50 Hz and the control-winding voltage remains constant, so V_{B1} is decreased with a slow slop caused by the power-winding voltage drop. Fig. 13 (c) and (f) indicate that V_{B2} is well regulated by the grid-connected converter and is constant during the speed rising and I_{B2} is increased so that the output power follows the power-speed curve. Fig. 13 proves the wide-speed-range generation for the proposed topology in which the boost converter is utilized by DWIG DC generation system.

The measured output power and efficiency of the system at different rotor speeds are illustrated in Fig. 14. The measured power is in agreement with the power-speed curve, defined in the controller. At low speeds, the power loss caused by the control-winding current for DWIG excitation is significant compared to the output power, therefore, the efficiency is low. At higher speeds, although the total power loss, including

copper loss, core loss, converter loss, and mechanical loss, is increased, but due to the higher output power the efficiency is higher. The maximum efficiency of the system is measured 78%. The efficiency curve can be improved in the systems with higher power rating because of the better generator parameters.

the whole operating speed range. Moreover, with a 77uF excitation capacitor, the control-winding current does not exceed 1.8 A within the speed range, as expected from the theoretical analysis. Thus, when the optimum excitation capacitor is selected, the maximum current of SEC is 1.8 A and the SEC capacity is limited to 710 VA.

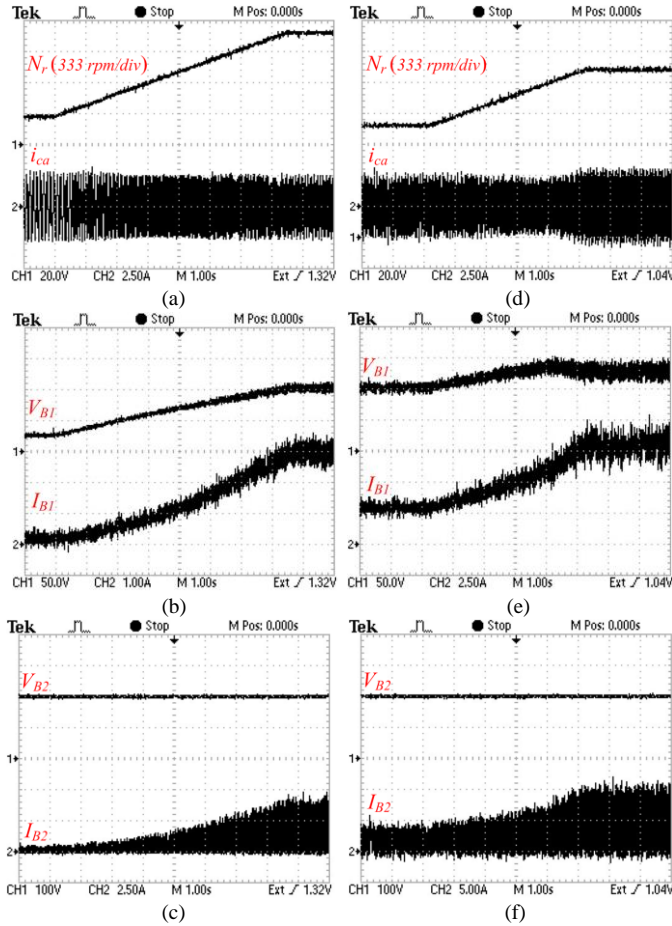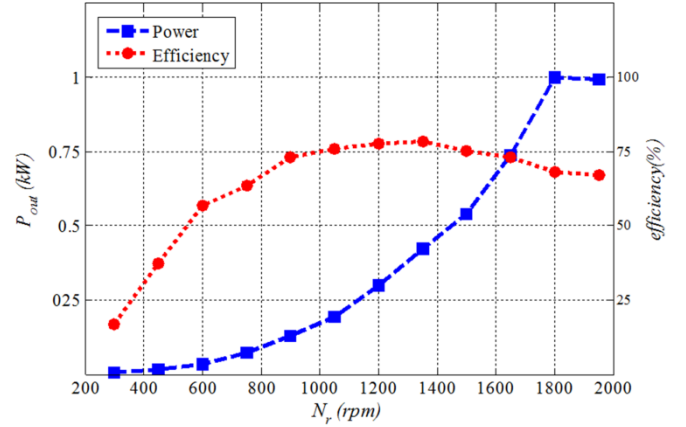Fig. 14. Experimental results for the output power and efficiency at different speeds.

Fig. 13. Experimental Result when the rotor speed is increased from 300 rpm to 1200 rpm ((a)-(c)) and from 1200 rpm to 1800 rpm ((d)-(f)).

Fig. 15 illustrates the control-winding line-to-line voltage and line current with/without excitation capacitor in 3 different speeds and loads (750 rpm, 72 W), (1350 rpm, 422W), (1800 rpm, 1 kW). In all figures, the current lags line-to-line voltage for about 120° which means the SEC provides only the reactive current for the DWIG excitation. The figures show the impact of the excitation capacitor on the reduction of the control winding current. In order to compare the calculated and the experimental results and also the effect of the optimum size of the capacitor (77 uF), the fundamental component of the control-winding current is extracted at different rotor speeds and loads.

Comparison between theoretical analysis and experimental results are illustrated in Fig. 16. In this figure, the solid lines denote the calculated results and the points denote the measured results of control-winding current, for the two conditions: with and without excitation capacitor. In both cases, the measured current has a good agreement with the theoretical results and both follow the same behavior within
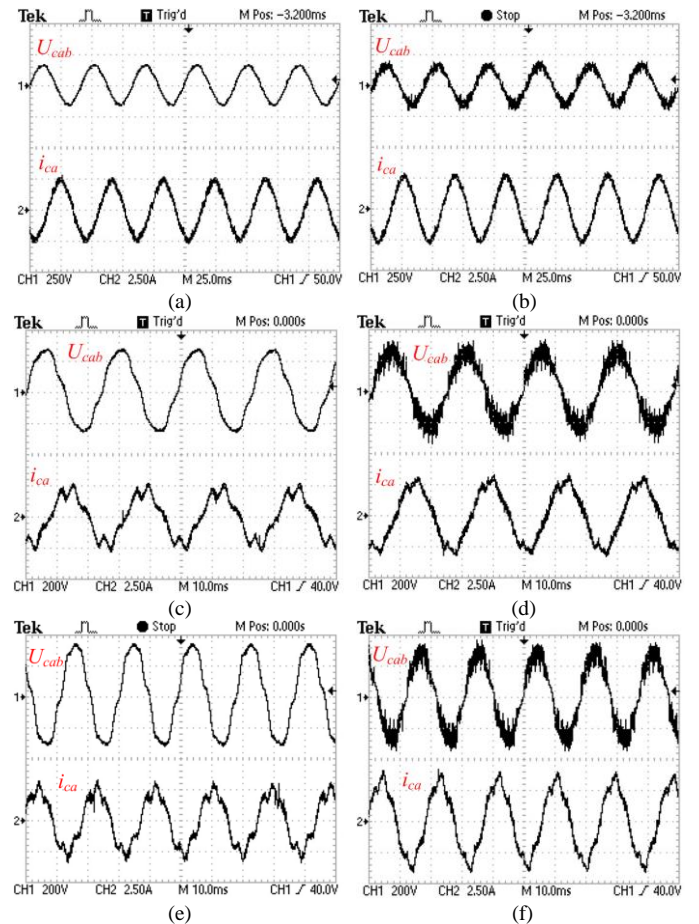

Fig. 15. Experimental result of the control winding voltage and current with and without C_{exc} at three different speeds and loads. a)750rpm/72W with C_{exc}. b)750rpm/72W without C_{exc}. c)1350rpm/422W with C_{exc}. d)1350rpm/422W without C_{exc}. e)1800rpm/1kW with C_{exc}. f)1800rpm/1kW without C_{exc}.

This article has been accepted for publication in a future issue of this journal, but has not been fully edited. Content may change prior to final publication. Citation information: DOI 10.1109/TPEL.2018.2797095, IEEE Transactions on Power Electronics
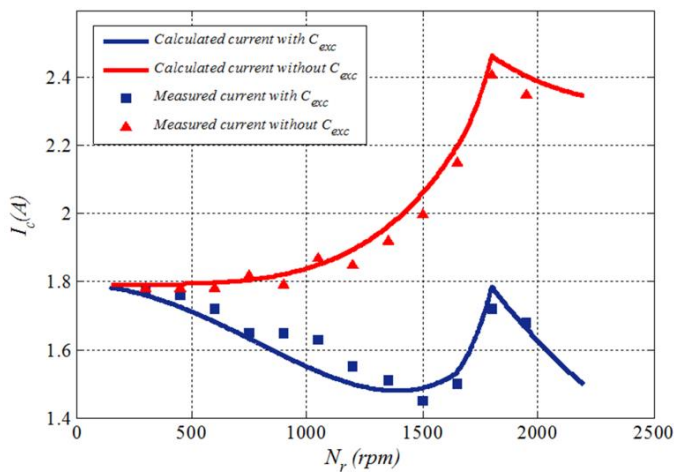
11

Fig. 16. Comparison between calculated and measured control-winding current and effect of the optimum excitation capacitor.

VIII. CONCLUSION

This paper proposes a topology for variable speed wind power application using dual stator-winding induction generator. A boost converter is utilized for MPPT and wide range variable speed operation, especially at low-speed condition is obtained. At low speeds, DWIG voltage is dropped due to *V/f* strategy and a boost converter is used to increase the voltage level to meet the higher and constant voltage requirement, such as in voltage source converter DC-link or offshore DC network applications. In the proposed topology, by choosing the optimum excitation capacitor, the capacity of the semiconductor excitation controller is minimized. Finally, to verify the proper operation of the proposed system, simulation and experimental results are presented which validate the wide-speed range operation of the system and the excitation capacitor optimization method.

REFERENCES

[1] REN21, "Renewables 2016: Global status report," 2016. [Online]. Available: http://www.ren21.net.

[2] F. Blaabjerg and K. Ma, "Future on Power Electronics for Wind Turbine Systems," *IEEE Journal of Emerging and Selected Topics in Power Electronics*, vol. 1, no. 3, pp. 139-152, Sept. 2013.

[3] Z. Chen, J. M. Guerrero, and F. Blaabjerg, "A Review of the State of the Art of Power Electronics for Wind Turbines," *IEEE Transactions on Power Electronics*, vol. 24, no. 8, pp. 1859-1875, Aug. 2009.

[4] V. Yaramasu, B. Wu, P. C. Sen, S. Kouro and M. Narimani, "High-power wind energy conversion systems: State-of-the-art and emerging technologies," *Proceedings of the IEEE*, vol. 103, no. 5, pp. 740-788, May 2015.

[5] H. Nian and Y. Song, "Direct Power Control of Doubly Fed Induction Generator Under Distorted Grid Voltage," *IEEE Transactions on Power Electronics*, vol. 29, no. 2, pp. 894-905, Feb. 2014.

[6] H. Li, and Z. Chen, "Overview of different wind generator systems and their comparisons," *IET Renew. Power Gener.*, vol. 2, no. 2, pp. 123-138, Jun. 2008.

[7] S. M. Muyeen, R. Takahashi, and J. Tamura, "Operation and Control of HVDC-Connected Offshore Wind Farm," *IEEE Transactions on Sustainable Energy*, vol. 1, no. 1, pp. 30-37, April 2010.

[8] N.M. Kirby, L. Xu, M. Luckett, and W. Siepmann, "HVDC transmission for large offshore wind farms," *Power Eng. J.*, vol. 16, no. 3, pp. 135-141, Jun. 2002.

[9] A. Egea-Alvarez, F. Bianchi, A. Junyent-Ferre, G. Gross, and O. Gomis-Bellmunt, "Voltage Control of Multiterminal VSC-HVDC Transmission Systems for Offshore Wind Power Plants: Design and Implementation in a Scaled Platform," *IEEE Trans. Ind. Electron.*, vol. 60, no. 6, pp. 2381-2391, Jun. 2013.

[10] S.V. Bozhko, R. Blasco-Gimenez, R. Li, J.C. Clare, and G.M. Asher, "Control of Offshore DFIG-Based Wind Farm Grid With Line-Commutated HVDC Connection," *IEEE Trans. Energy Conversion*, vol. 22, no. 1, pp.71-78, Mar. 2007.

[11] J. Hu, J. Zhu, Y. Zhang, G. Platt, Q. Ma, and D. G. Dorrell, "Predictive Direct Virtual Torque and Power Control of Doubly Fed Induction Generators for Fast and Smooth Grid Synchronization and Flexible Power Regulation," *IEEE Trans. Power Electronics*, vol.28, no.7, pp. 3182-3194, Jul. 2013.

[12] A. I. Andrade, R. Blasco-Gimenez and G. R. Pena, "Distributed control strategy for a wind generation systems based on PMSG with uncontrolled rectifier HVDC connection," in *IEEE International Conference on Industrial Technology (ICIT)*, Seville, 2015, pp. 982-986.

[13] F. Bu, W. Huang, Y. Hu, K. Shi, "Control and Implementation of Dual Stator-Winding Induction Generator for Variable Frequency AC-Generating System," *Journal of Power Electronics*, vol. 13, no. 5, pp. 798-805, Sept. 2013.

[14] J. A. Barrado-Rodrigo, J. I. Talpone, and L. Martinez-Salamero, "Variable-speed wind energy conversion system based on a dual stator-winding induction generator," in *IET Renewable Power Generation*, vol. 11, no. 1, pp. 73-80, 1 11 2017.

[15] S. Basak and C. Chakraborty, "Dual Stator Winding Induction Machine: Problems, Progress, and Future Scope," in *IEEE Transactions on Industrial Electronics*, vol. 62, no. 7, pp. 4641-4652, July 2015.

[16] H. Xu, F. Bu, W. Huang, Y. Hu and H. Liu, "Control and Performance of Five-Phase Dual Stator-Winding Induction Generator DC Generating System," in *IEEE Transactions on Industrial Electronics*, vol. 64, no. 7, pp. 5276-5285, July 2017.

[17] F. Bu, Y. Hu, W. Huang, S. Zhuang and K. Shi, "Control Strategy and Dynamic Performance of Dual Stator-Winding Induction Generator Variable Frequency AC Generating System With Inductive and Capacitive Loads," in *IEEE Transactions on Power Electronics*, vol. 29, no. 4, pp. 1681-1692, April 2014.

[18] S. Basak and C. Chakraborty, "A New Optimal Current Control Technique for Dual Stator Winding Induction Generator," in *IEEE Journal of Emerging and Selected Topics in Power Electronics*, vol. 5, no. 2, pp. 820-832, June 2017.

[19] H. Xu, F. Bu, W. Huang, Y. Hu, and Y. Zhao, "Analysis, Comparison, and Discussion of Control Strategies for Dual Stator-Winding Induction Generator DC Generating System," *IEEE Journal of Emerging and Selected Topics in Power Electronics*, vol. 4, no. 3, pp. 1007-1014, Sept. 2016.

[20] F. Bu, Y. Hu, W. Huang and S. Zhuang, "Parameter Design and Static Performance of Dual Stator-Winding Induction Generator Variable Frequency AC Generating System With Inductive and Capacitive Loads," in *IEEE Transactions on Industrial Electronics*, vol. 61, no. 8, pp. 3902-3914, Aug. 2014.

[21] Y. Li, Y. Hu, W. Huang, L. Liu, and Y. Zhang, "The Capacity Optimization for the Static Excitation Controller of the Dual-Stator-Winding Induction Generator Operating in a Wide Speed Range," *IEEE Transactions on Industrial Electronics*, vol. 56, no. 2, pp. 530-541, Feb. 2009.

[22] F. Bu, S. Zhuang, W. Huang, N. Su, and Y. Hu, "Asymmetrical Operation Analysis for Dual Stator-Winding Induction Generator Variable Frequency AC Generating System With Unbalanced Loads," in *IEEE Transactions on Industrial Electronics*, vol. 64, no. 1, pp. 52-59, Jan. 2017.

[23] M. Moradian and J. Soltani, "An Isolated Three-Phase Induction Generator System With Dual Stator Winding Sets Under Unbalanced Load Condition," in *IEEE Transactions on Energy Conversion*, vol. 31, no. 2, pp. 531-539, June 2016.

[24] M. Hassan Zamani, G. Hossein Riahy, and M. Abedi, "Rotor-Speed Stability Improvement of Dual Stator-Winding Induction Generator-Based Wind Farms By Control-Windings Voltage Oriented Control," *IEEE Transactions on Power Electronics*, vol. 31, no. 8, pp. 5538-5546, Aug. 2016.

[25] O. Ojo and I. E. Davidson, "PWM-VSI inverter-assisted stand-alone dual stator winding induction generator," *IEEE Transactions on Industry Applications*, vol. 36, no. 6, pp. 1604-1611, Nov/Dec 2000.

[26] Li Yong, H. Yuwen, L. Lingshun, H. Wenxin and C. Guanghui, "Control of a Novel Dual Stator-Winding Induction Generator for wide speed-range operation," *2007 IEEE Power Electronics Specialists Conference*, Orlando, FL, 2007, pp. 2096-2101.

[27] L. Yong, H. Yuwen, H. Wenxin, L. Lingshun, C. Guang-hui and Q. Jingfeng, "The Dual Stator-Winding Induction Generator for Wide-Speed-Range Operation," *2007 International Conference on Clean Electrical Power*, Capri, 2007, pp. 619-624.

[28] F. Bu, W. Huang, Y. Hu and K. Shi, "An Excitation-Capacitor-Optimized Dual Stator-Winding Induction Generator With the Static Excitation Controller for Wind Power Application," *IEEE Transactions on Energy Conversion*, vol. 26, no. 1, pp. 122-131, March 2011.

[29] F. Bu, Y. Hu, W. Huang, S. Zhuang and K. Shi, "Wide-Speed-Range-Operation Dual Stator-Winding Induction Generator DC Generating System for Wind Power Applications," in *IEEE Transactions on Power Electronics*, vol. 30, no. 2, pp. 561-573, Feb. 2015.

[30] K. Shi, P. Xu, Z Wan, F. Bu, Z. Fang, R. Liu, and D. Zhao, "Grid-Connected Dual Stator-Winding Induction Generator Wind Power System for Wide Wind Speed Ranges," *Journal of Power Electronics*, vol. 16, no. 4, pp. 1455-1468, July 2016.

[31] R. Sharma, T. W. Rasmussen and B. B. Jensen, "Application of a synchronous generator with a boost converter in wind turbines: an experimental overview," *IET Renewable Power Generation*, vol. 6, no. 6, pp. 414-423, November 2012.

[32] M. E. Haque, M. Negnevitsky, and K. M. Muttaqi, "A Novel Control Strategy for a Variable-Speed Wind Turbine With a Permanent-Magnet Synchronous Generator," *IEEE Transactions on Industry Applications*, vol. 46, no. 1, pp. 331-339, Jan.-Feb. 2010.

[33] V. Yaramasu, B. Wu, M. Rivera and J. Rodriguez, "A New Power Conversion System for Megawatt PMSG Wind Turbines Using Four-Level Converters and a Simple Control Scheme Based on Two-Step Model Predictive Strategy—Part I: Modeling and Theoretical Analysis," *IEEE Journal of Emerging and Selected Topics in Power Electronics*, vol. 2, no. 1, pp. 3-13, March 2014.

[34] R. M. Linus and P. Damodharan, "Maximum power point tracking method using a modified perturb and observe algorithm for grid connected wind energy conversion systems," *IET Renewable Power Generation*, vol. 9, no. 6, pp. 682-689, Aug. 2015.

[35] Paul C. Krause, Oleg Wasynczuk, Scott D. Sudhoff, Steven Pekarek, *Analysis of Electric Machinery and Drive Systems*, 3rd ed., Piscataway, NJ, USA: Wiley-IEEE Press, 2013, pp.1-52.

[36] M. P., "Theory (Instantaneous Power Theory and Applications to Power Conditioning; Akagi, H. et al; 2007) [Book Review]," *IEEE Industrial Electronics Magazine*, vol. 1, no. 3, pp. 46-46, Fall 2007.

[37] Bin Wu, Yongqiang Lang, Navid Zargari, Samir Kouro, "Appendix B: Generator Parameters," in *Power Conversion and Control of Wind Energy Systems*, 1st ed., Hoboken, NJ, USA: Wiley-IEEE Press, 2011, pp. 319-326.